Journal of Nuclear Materials 393 (2009) 481–486

Contents lists available at ScienceDirect

Journal of Nuclear Materials

journal homepage: www.elsevier.com/locate/jnucmat

Response of synthetic coffinite to energetic ion beam irradiation

J. Lian [a,*], J.M. Zhang [b], V. Pointeau [b], F.X. Zhang [b], M. Lang [b], F.Y. Lu [a], C. Poinssot [c], R.C. Ewing [b,*]

[a] Department of Mechanical, Aerospace and Nuclear Engineering, Rensselaer Polytechnic Institute, Troy, NY 12180, United States
[b] Department of Geological Sciences, University of Michigan, Ann Arbor, MI 48109, United States
[c] Nuclear Energy Division, Department of Radiochemistry and Processes, Commissariat à l'Energie Atomique, CEA Marcoule, 30200 Bagnols-Sur-Cèze cedex, France

ARTICLE INFO

Article history:
Received 14 April 2009
Accepted 13 July 2009

ABSTRACT

Coffinite, $USiO_4$, is one of the two most abundant and important naturally occurring U^{4+} phases (the other is UO_2), and it is an alteration product of the UO_2 in spent nuclear fuel when in contact with silica-rich groundwater under reducing conditions. Despite its ubiquity, there are very limited data on the response of coffinite to radiation. Here, we present the results of the first systematic investigation of energetic ion beam irradiation (1 MeV Kr^{2+}) of ultra-fine, synthetic coffinite (20–50 nm). *In situ* transmission electron microscopy (TEM) showed that the crystalline-to-amorphous transformation occurs at a relatively low dose, ~0.27 displacements per atom (dpa) at room temperature. The critical temperature, T_c, above which coffinite cannot be amorphized, is low (~608 K). Synthetic coffinite is more stable as compared with isostructural zircon ($ZrSiO_4$; T_c = 1000 K) and thorite ($ThSiO_4$; T_c above 1100 K) upon ion beam irradiation at elevated temperature, suggesting enhanced defect annealing behavior in nano-sized synthetic coffinite. Irradiation was found to decrease the temperature required to induce phase decomposition process in coffinite upon thermal annealing. A good correlation among the critical amorphization temperature, T_c, phase decomposition temperature, T_f, and the temperature range of the two-phase (ZrO_2 and SiO_2) co-existed region was identified.

1. Introduction

Actinide-bearing phases are inevitably exposed to radiation damage due to alpha-decay events. In natural minerals, such as coffinite, $USiO_4$, significant radiation doses, tens of displacements per atom, dpa, accumulate over geologic periods. Coffinite occurs as a common alteration product of uraninite, UO_{2+x}, a natural analogue to the UO_2 in spent nuclear fuel [1–3]. Coffinite will form as an alteration product of spent nuclear fuel exposed to silica-rich ground water under reducing conditions [4–9]. The radiation response of coffinite is of even greater interest if it also incorporates transuranium elements, such as Pu, during the corrosion of UO_2 in spent nuclear fuel, particularly a mixed oxide fuel [10,11].

Coffinite ($I4_1/amd$, $Z = 4$) is an orthosilicate, isostructural with zircon ($ZrSiO_4$), hafnon ($HfSiO_4$), thorite ($ThSiO_4$) [12–15], and other actinide silicates in which the actinides (e.g., Np, Pu, Am) are typically in the 4^+ valence state [16,17]. Pu^{3+} substitutes into zircon synthesized under reducing conditions [18]. The A-site, which contains uranium, is surrounded by eight oxygens: four at a distance of 0.238 nm and four at the distance 0.236 nm, distances comparable to those in UO_2 (0.236 nm) [19]. The coffinite structure consists of a chain of alternating, edge-sharing SiO_4 tetrahedra and UO_8 (or ThO_8) triangular dodecahedra extending parallel to the *c*-axis [17,20].

The phase stability and response of the isostructural orthosilicates including zircon, hafnon, and thorite under intense radiation fields have been studied extensively by ion beam irradiations combined with *in situ* TEM observation [21–24]. All of these orthosilicates experience a radiation-induced crystalline-to-amorphous transformation at room temperature at relatively low doses (0.17–0.22 dpa) and can be amorphized even at temperatures up to 1000 K [21]. However, no irradiation data are available for the uranium end-member, coffinite, because the synthesis of coffinite has proven to be very difficult. In this study, we have performed ion beam irradiations on synthetic coffinite with a crystal size in the range of 20–50 nm, consistent with the ultra-fine nature of the coffinite as it forms as an alteration product of spent nuclear fuel or occurs in natural uranium deposits. The results of the systematic ion beam irradiations of coffinite are compared with previous results for isostructural zircon, hafnon and thorite. The synthetic nanocrystalline coffinite is more stable than bulk zircon and thorite at elevated temperatures; however, the enhanced radiation performance may be related to the very fine particle size of the coffinite, as the very small grain size may allow for more rapid annealing of defects as they are annihilated at the grain surfaces.

* Corresponding authors.
E-mail addresses: lianj@rpi.edu (J. Lian), rodewing@umich.edu (R.C. Ewing).

0022-3115/$ - see front matter © 2009 Elsevier B.V. All rights reserved.
doi:10.1016/j.jnucmat.2009.07.005

2. Experimental

The synthetic coffinite ($USiO_4$) was prepared from solutions of UCl_4 and Na_2SiO_3 during reaction in an autoclave under hydrothermal conditions (250 °C, 40 bars). The details of the synthesis method are described in Pointeau et al. [25]. XRD measurements confirmed that the synthesized powder was tetragonal coffinite, isostructural with zircon; however, varying amounts of poorly–crystalline impurities were detected by EMPA analyses (mainly UO_2 and SiO_2 gel). TEM analysis, using selected area electron diffraction (SAED) patterns, confirmed the presence of coffinite, consistent with the XRD measurements (Fig. 1(a)). TEM samples were prepared by dispersing as-synthesized powders on holy carbon grids suitable for direct microstructural characterization and ion beam irradiations. Bright-field and high resolution TEM (HRTEM) images (Fig. 1(a) and (b)) showed that the as-synthesized samples consisted of well crystallized powders with facets, and the grain size was in the range of 20–50 nm (Fig. 1(b)).

The radiation response of synthetic coffinite was investigated by 1 MeV Kr^{2+} irradiation. Ion irradiation and *in situ* TEM observations were performed using the IVEM-Tandem Facility at the Argonne National Laboratory from room temperature to 623 K. During irradiation, the ion beam was aligned approximately normal to the sample surface. The ion flux was 6.25×10^{11} ions/cm^2 s. The crystalline-to-amorphous transformation was observed intermittently by observing the SAED pattern and by *in situ* HRTEM imaging. The critical amorphization fluence (F_c), at which complete amorphization occurs, was experimentally determined by noting the fluence at which all of the diffraction maxima disappeared in the SAED patterns. Different grains of coffinite were monitored during the ion irradiations, and final doses were obtained by averaging the experimental data of typically more than 10 grains. Before the irradiation, the powdered samples were heated at the desired temperature for 30 min in order to achieve a more uniform temperature. Furthermore, different grains, either attached or close to the copper grid, were selected for investigation in order to minimize the uncertainty in temperature. The critical amorphization fluence, F_c, in ions/cm^2 was converted to critical dose, D_c, in the unit of displacements per atom (dpa) using SRIM-2008 full cascade simulations. No displacement energies, E_d, are available for coffinite; thus, the displacement energies for zircon, 79 eV (A-site cation), 23 eV (Si), and 47 eV (O) [26,27], were used for the SRIM-2008 calculation for coffinite in order to compare its behavior with the results for zircon and thorite in previous studies [21–23].

3. Results and discussion

A sequence of SAED patterns of synthetic coffinite subjected to 1 MeV Kr^{2+} at different doses at room temperature are shown in Fig. 2. The polycrystalline ring patterns, characteristic of nanostructured materials, gradually faded with increasing radiation fluence, and complete amorphization occurred at a dose of 0.27 dpa, as shown in Fig. 2(d) in which only diffuse halos in the diffraction pattern were observed. *In situ* HRTEM images (Fig. 3) of a coffinite particle viewed along [1–11] zone axis clearly show the disruption of the lattice fringes with increasing dose. The lattice fringes are almost entirely lost at a dose of ~0.38 dpa. The relatively high dose for this particular particle, as compared with the critical value (0.27 dpa) determined from SAED pattern (Fig. 2(d)), can be attributed to the channeling effects along the zone axis, causing less en-

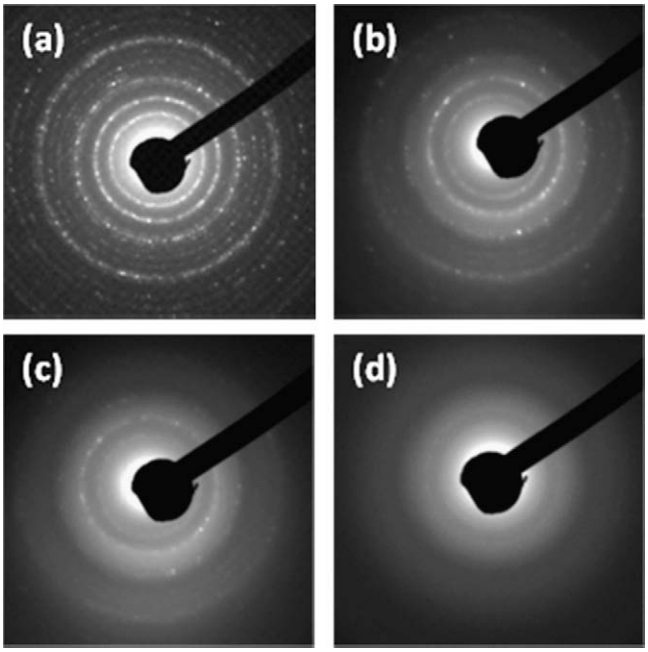

Fig. 2. A sequence of SAED patterns of synthetic coffinite subject to 1 MeV Kr^{2+} irradiation at room temperature at different doses: (a) unirradiated, (b) 0.13, (c) 0.21, and (d) 0.28 dpa. The critical amorphization dose at room temperature can be determined as ~0.28 dpa.

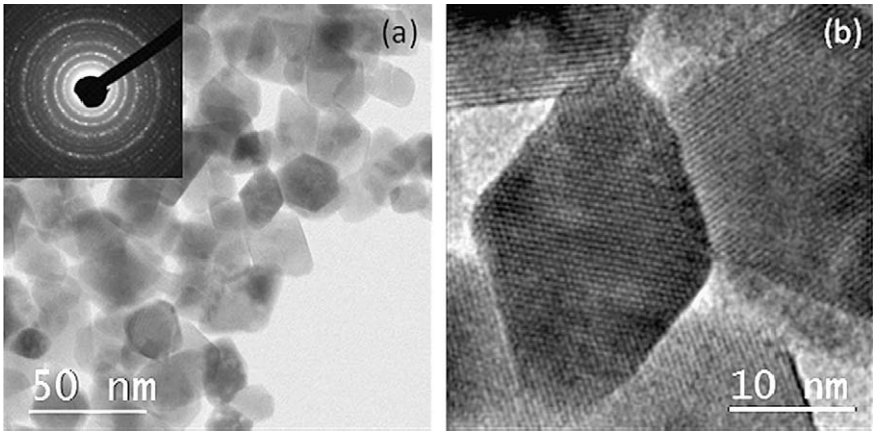

Fig. 1. Bright-field (a) and high resolution TEM (b) images showing the size, morphology, and structure of synthetic nano-sized coffinite. Inset is a SAED pattern, consistent with tetragonal coffinite.

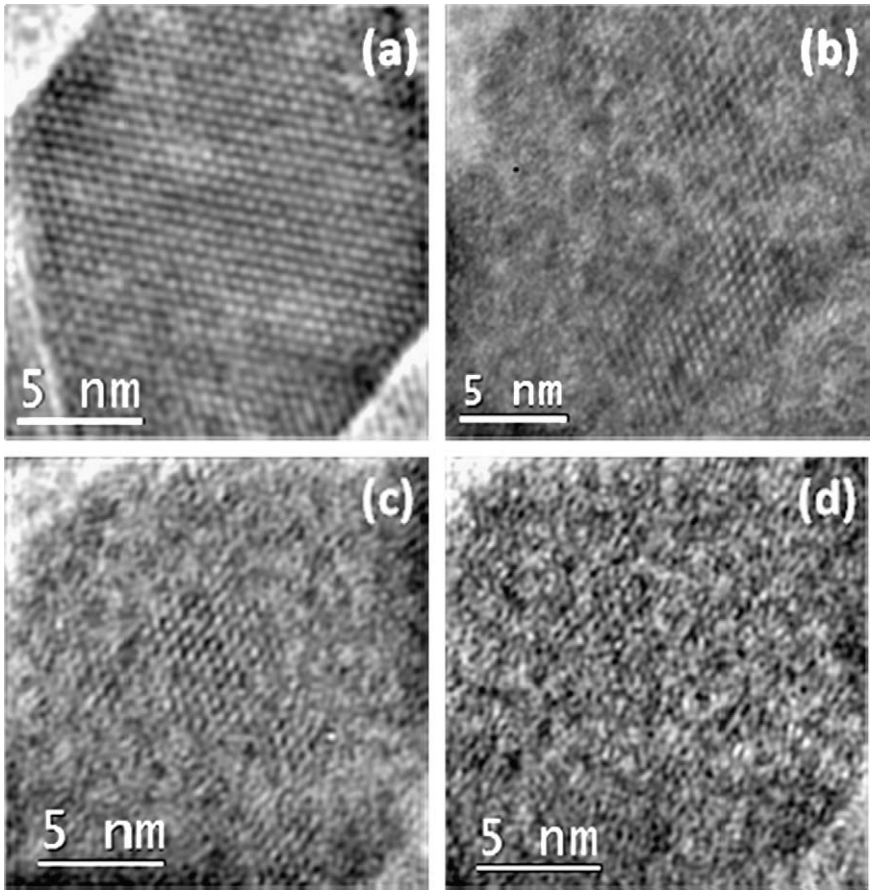

Fig. 3. *In situ* HRTEM images showing the evolution of a coffinite nanoparticle along [1–11] zone axis as a function of radiation doses: (a) 0, (b) 0.21, (c) 0.33, and (d) 0.38 dpa.

ergy to be transferred to target atoms. In addition to the radiation-induced, crystalline-to-amorphous structural transition, we also found that the facets of the synthetic coffinite nanoparticles disappeared, and the resulting amorphous particles were rounded in shape. The combination of SAED patterns and *in situ* HRTEM images indicated that the structure and morphology of synthetic coffinite are sensitive to radiation damage at room temperature. The critical amorphization dose is slightly higher than those of zircon (0.17 dpa), hafnon (0.22 dpa) and thorite (0.16 dpa) upon 800 keV Kr^{+} ion irradiation [16]. Considering that lower amounts of nuclear energy loss caused by higher energy bombardment in coffinite, the radiation response of ultra-fine coffinite particles is similar to that of isostructural zircon, hafnon and thorite, and the critical amorphization doses at room temperature are within experimental error.

Irradiation-induced amorphization is a dynamic balance between irradiation-induced defect production and defect recovery processes. Fig. 4 shows the temperature dependence of ultra-fine coffinite subjected to 1 MeV Kr^{2+} irradiation. The critical amorphization dose increases at elevated temperatures due to dynamic annealing. Based on a direct impact model [28,29], the temperature dependence of amorphization dose, D_c, can be expressed by:

$$D_c = \frac{D_0}{1 - \exp[(E_a/k)((1/T_c) - (1/T)]}, \quad (1)$$

where D_0 is the amorphization dose extrapolated to absolute zero – the point at which no annealing can occur. E_a is the activation energy for the dynamic annealing process during irradiation; T_c is the critical amorphization temperature above which amorphization cannot occur. Based on Eq. (1), the critical amorphization temperature, T_c, and activation energy of recrystallization, E_a, can be determined (Table 1). However, the calculated activation energy is strongly dependent on the model used to fit the curve of the temperature dependence of the critical amorphization dose (Fig. 4), and significant uncertainty can be introduced depending on the damage accumulation model that is used [30]. Thus, these calculated activation energies are less useful than the critical amorphization temperature, T_c, in evaluating a material's 'susceptibility' to radiation-induced amorphization.

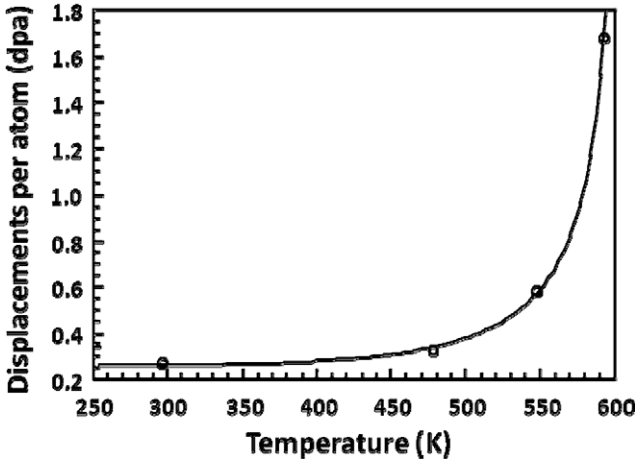

Fig. 4. Temperature dependence of radiation-induced amorphization of synthetic coffinite subject to 1 MeV Kr^{2+}. The critical amorphization temperature was determined to be 608 K.

Table 1
The ratio of electronic to nuclear stopping power (ENSP) based on a full cascade calculation using SRIM-2008, critical amorphization fluence and dose at room temperature, calculated activation energy, E_a, and critical amorphization temperature, T_c, phase decomposition temperature, T_f, from amorphous matrix, and the temperature range of the two-phase region based on corresponding phase diagrams for coffinite (this study) and isostructural orthosilicates [16].

Compound	Irradiation source	ENSP	F_c (10^{14} ions/cm^2)	D_c (dpa)	Activation energy (eV)*	T_c (K)	T_f (K)	Two-phase co-existence region (K)
Zircon	800 keV Kr^+	1.09	1.48	0.17	3.3	1000	900	1960–2675
Hafnon	800 keV Kr^+	1.21	1.50	0.22	3.5	1070	950	2025–2875
Thorite	800 keV Kr^+	1.10	1.15	0.16	>3.6	>1100	1000	2250–2475
Coffinite	1 MeV Kr^{2+}	1.19	2.06	0.28	0.28	608	573*	>673

* Thermally-induced phase decomposition occurred in amorphous coffinite. Activation energy for defect annealing and critical amorphization temperature was derived based on a two-stage model for other orthosilicates [16].

The critical amorphization temperature, T_c, above which complete amorphization cannot be achieved, was determined to 608 ± 1 K for synthetic coffinite upon 1 MeV Kr^{2+} irradiation, significantly lower than that of isostructural zircon, hafnon and thorite upon 800 keV Kr^+ irradiation. The critical amorphization temperatures for bulk zircon, hafnon and thorite are 1000, 1070 and above 1100 K, respectively [21]. The calculated activation energy for the dynamic defect annealing for coffinite subjected to 1 MeV Kr^{2+} irradiation is low (0.28 ± 0.01 eV), as compared with 3.3 eV for $ZrSiO_4$ and 3.1 eV for $ThSiO_4$ [21]. Although coffinite appears to be as sensitive to radiation damage as isostructural zircon, hafnon and thorite at lower temperatures, the defect recovery efficiency for coffinite at elevated temperatures is greater than that of zircon, hafnon and thorite. Based on their critical amorphization temperatures, the resistance of these isostructural orthosilicates to ion irradiation-induced amorphization can be ranked (most stable to least stable) as: nano-sized coffinite > bulk zircon and hafnon > bulk thorite.

The large difference in the radiation response at elevated temperatures reflects a fundamental difference in the amorphization and recrystallization kinetics between coffinite and the other isostructural orthosilicates. Various empirical factors have been employed to explain the radiation response of complex ceramics, such as the cation size [31], structural connectivity [32], ionicity [33] and the original degree of disorder [34]. For orthosilicates, e.g., $ThSiO_4$, huttonite with a monoclinic structure displays a greater resistance to amorphization than tetragonal thorite. Similarly, radiation damage can be easily annealed in the monazite structure-type, as compared with the zircon structure-type [30]. The tetragonal orthophosphate is more resistant to radiation damage than orthosilicates, suggesting that the chemical composition and degree of polymerization can have a significant effect on the radiation response of complex ceramics [30]. Because coffinite is isostructural with zircon, hafnon and thorite, we expected that radiation-induced amorphization should occur at roughly similar fluencies. It has also been reported that the critical amorphization temperature increases with higher mass of the cations for a number of phases of variable composition: pyrochlore [35], perovskite [36], monazite and zircon-type structures [30]. The structure-type, ABO_4, with heavier A-site cation mass has a higher amorphization temperature [30]. Thus, based on the mass difference, coffinite with the heaviest cation ($m_U > m_{Zr,Hf}$) should be more susceptible to ion-beam-induced amorphization; however, our results clearly indicate that the critical amorphization temperature for synthetic nano-sized coffinite is actually much lower than those of bulk zircon and hafnon.

The ion beam conditions (ion mass and energy) significantly influence the damage process (e.g., low energy heavier ions create a large cascade size with less defect annealing), and thus the critical amorphization temperature. As an example, for the zircon structure, the critical amorphization temperature upon 1.5 MeV Xe^+ irradiation is 1040 K, slightly higher than that of 800 keV Kr^+ [16]. The ratio of electronic to nuclear stopping power (ENSP) has been found to correlate well with the amorphization resistance for some complex ceramics including the orthosilicate phases [30]. Ionizing radiation may promote the annealing and recrystallization of the amorphous domains, leading to greater amorphization resistance. Based on full cascade calculations using SRIM-2008 with exactly the same displacement energies for coffinite, zircon and thorite, the ENSP ratio for coffinite upon 1 MeV Kr^{2+} is similar to that of zircon and thorite subjected to the 800 keV Kr^+ ion irradiation (see Table 1). This comparison suggests that the ion mass, structure, composition, bond-type and ENSP cannot explain the greater amorphization resistance of ultra-fine coffinite as compared with isostructural bulk zircon and thorite.

The greater amorphization resistance of this synthetic coffinite may be related to the fact that the individual crystals are nanometers in size. Nanostructured materials can display a dramatically different behavior under intense radiation fields as compared with their bulk counterparts. Specifically, nanostructured materials have a high surface-to-volume ratio, and the greater surface area may provide sinks for point defects and defect cluster annihilation. As the size of a crystal decreases to the nano-scale regime, below a critical value, comparable to the characteristic diffusion length of defects, defects may be easily annihilated. Previous studies have reported the enhanced radiation performance for nanostructured materials. For example, a large increase in the amorphization resistance was reported for single-phase nanocrystalline spinel as compared with a polycrystalline aggregate [37]. A nanocrystalline $Ti_{49.4}Ni_{50.6}$ alloy with a grain size of 23–31 nm retained its long-range order, while its coarse-grained counterpart was amorphized at the same dose upon 1.5 MeV Ar^+ ion irradiation at room temperature [38]. We have also recently reported a greatly-enhanced radiation resistance for nanocrystalline pyrochlore [39].

The increasing resistance to ion-beam-induced amorphization at elevated temperatures in nano-sized coffinite, as compared with bulk zircon and thorite further underscores the importance of crystal size in controlling phase stability, and thus, materials performance in an irradiation environment. On the other hand, the ultra-fine coffinite displayed a similar radiation response at room temperature, comparable to that of bulk zircon and thorite, suggesting that the defect production processes are similar and no significant annealing occurred at room temperature, for which the defects may have lower mobility. With increasing irradiation temperature, defects will recover quickly in nanostructured coffinite, as compared with bulk zircon and thorite, leading to dramatically increased amorphization doses. Above the critical amorphization temperature, all of the defects created by energetic beam irradiations are annealed; thus, no amorphization can occur. The interplay among defect production and annealing, temperature and crystal size is important in predicting materials performance under intense radiation fields.

Zircon and hafnon have been shown to decompose upon ion beam irradiations at temperatures close or above the critical amorphization temperature, at which materials decompose into component oxide nanoparticles (ZrO_2 or HfO_2) and silica-rich, SiO_2,

domains [20–22]. The phase decomposition occurs in the amorphous matrix at temperatures above 900 K for $ZrSiO_4$ and ~950 K for $HfSiO_4$ upon continuous irradiation, and it can directly occur in crystalline matrix upon irradiation at temperatures above T_c without the formation of the intermediate amorphous phase [20]. A similar radiation-induced decomposition was observed in amorphous $ThSiO_4$ irradiated above 1000 K [21]; however, it did not decompose directly to the component oxides at the highest obtainable temperature (1100 K). The formation of ZrO_2 and HfO_2 did not occur in pre-amorphized $ZrSiO_4$ upon thermal annealing at a temperature of 1100 K as well. At a higher temperature of 1275 K, the phase decomposition to ZrO_2 and silica occurred in amorphous Pu-zircon and amorphous (metamict) natural zircons [40].

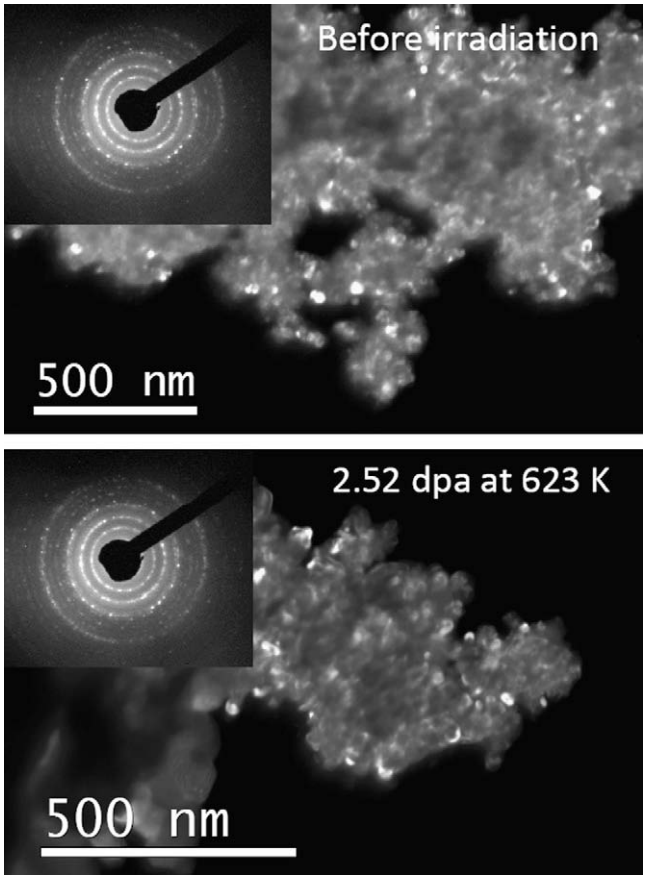

Fig. 5. Bright-field TEM images and corresponding SAED patterns show the morphology and structure of synthetic coffinites at 623 K before and after irradiation at a dose of 2.52 dpa. No direct phase decomposition occurred upon thermal annealing or ion beam irradiation at 623 K.

The irradiation-induced phase decomposition of zircon and hafnon has been explained by the thermal spike mechanism [41], by which the high-energy irradiation creates a 'liquid-like' state within displacement cascades. A crystalline ZrO_2 phase may coexist with a silica-rich liquid phase within temperature range of 1960 and 2675 K based on the ZrO_2–SiO_2 phase diagram [42]. Irradiation at elevated temperature may allow the nucleation of crystalline ZrO_2 by decreasing the cooling rate at temperatures of the two-phase region upon cascade quenching, leading to precipitation and phase decomposition. Comparing the phase decomposition behaviors of $ZrSiO_4$, $HfSiO_4$ and $ThSiO_4$, the phase decomposition temperature correlates with the temperature region within which two-phases coexist based on the corresponding phase diagrams [21].

Unlike $ZrSiO_4$ and $HfSiO_4$, for synthetic coffinite, no chemical decomposition of the crystalline matrix was observed upon irradiations at 623 K, slightly above the critical amorphization temperature, and the coffinite structure persisted to a dose of 2.52 dpa (see Fig. 5). The morphology (e.g., shape and size) of synthetic coffinite remained unchanged. Instead, upon thermal annealing at 573 K in less than 30 min, slightly below the critical amorphization temperature, recrystallization occurred and random distributed nanoparticles formed. By indexing FFT image of the high resolution TEM images, both coffinite and uraninite nanocrystals were found to be co-existed (Fig. 6). This result suggests that phase decomposition process may occur in amorphous coffinite domains upon thermal annealing at a temperature as low as 573 K, leading to the formation of UO_2 nanocrystals and SiO_2-rich zones. Naturally occurring coffinite has been reported to decompose into UO_2 and amorphous silica when heated above 673 K [43]. The same study has reported that synthetic coffinite is thermally stable in a vacuum for at least 5 h at 973 K [43]. Therefore, the two-phase (UO_2 and amorphous silica) region is expected to be more stable as compared with those of synthetic coffinite for temperatures higher than 673 K. The lower phase decomposition temperature in pre-amorphized coffinite in this study, than these of natural and synthetic coffinite upon thermal annealing, suggests that defect production and accumulation due to radiation damage may decrease

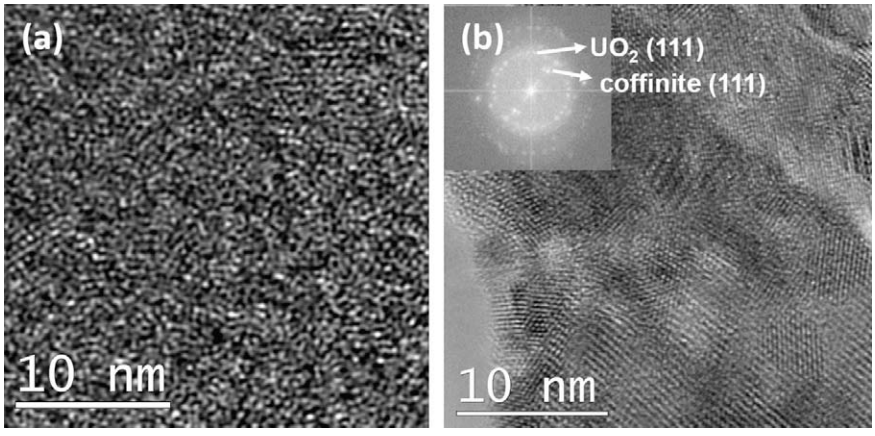

Fig. 6. High resolution TEM images show thermal annealing-induced recrystallization (b) at 573 K from pre-amorphized coffinite (a) created by 1 MeV Kr^{2+} irradiation at room temperature at a dose of 0.38 dpa. The co-existence of coffinite and uraninite nanocrystals as indexed from the FFT image (inset in Fig. 5b) suggests that, in addition to thermally-induced recrystallization, phase decomposition also occurs in amorphous coffinite at 573 K, leading to the formation of UO_2 nanocrystals.

the stability and enhance the phase decomposition processes of coffinite. The enhanced self diffusion in an amorphous state as compared with crystalline materials may accelerate the phase decomposition process in synthetic coffinite. By comparing the irradiation and thermal annealing results for coffinite, zircon, hafnon and thorite, we demonstrate that there might be a good correlation among the critical amorphization temperature, T_c, phase decomposition temperature, T_f, and the temperature range of the two-phase (ZrO_2 and SiO_2) co-existed region (Table 1).

4. Conclusions

In summary, we report the first irradiation results for synthetic coffinite and compare its behavior in a radiation field to that of isostructural zircon, hafnon and thorite. The dose required for amorphization of nanocrystals of coffinite at room temperature is similar to that of bulk zircon, hafnon and thorite. However, coffinite has a greater resistance to amorphization at elevated temperatures. The lower critical amorphization temperature for nanosized coffinite provides an important example of nanostructured materials having enhanced performance in intense irradiation fields. Amorphous coffinite rapidly recrystallized back to coffinite and uraninite nanocrystals upon thermal annealing at 573 K, and the lower phase decomposition temperature for pre-amorphized coffinite as compared with that of synthetic and natural coffinite suggests that radiation-induced amorphization may decrease the energy barrier to phase decomposition.

Acknowledgements

This work was supported by the Office of Basic Energy Sciences of the US Department of Energy (DE-FG02-97ER45656 and DE-FG02-06ER15783) and by the Commissariat à l'Energie Atomique. The authors also acknowledge the assistance of the staff of IVEM-Tandem Facility at Argonne National Laboratory during ion irradiation and *in situ* TEM observation.

References

[1] J. Janeczek, R.C. Ewing, V.M. Oversby, L.O. Werme, J. Nucl. Mater. 238 (1996) 121.
[2] J. Janeczek, R.C. Ewing, Geochim. Cosmochim. Acta 59 (1995) 1917.
[3] M. Fayek, T.M. Harisson, R.C. Ewing, M. Grove, C.D. Coath, Chem. Geol. 185 (2002) 205.
[4] M.B. Goldhaber, B.S. Hemingway, A. Mohagheghi, R.L. Reynolds, H.R. Northrop, Bull. Minéral. 110 (1987) 131.
[5] G. Smits, Can. Mineral. 27 (1989) 643.
[6] J. Janeczek, R.C. Ewing, Mater. Res. Soc. Symp. Proc. 257 (1992) 497.
[7] J. Janeczek, R.C. Ewing, J. Nucl. Mater. 190 (1992) 157.
[8] V. Savary, M. Pagel, Geochim. Cosmochim. Acta 61 (1997) 4479.
[9] R. Bros, H. Hidaka, T. Ohnuki, Appl. Geochem. 18 (2003) 1807.
[10] A.P. Deditius, S. Utsunomiya, R.C. Ewing, Chem. Geol. 251 (2008) 33.
[11] A.P. Deditius, S. Utsunomiya, M.A. Wall, V. Pointeau, R.C. Ewing, Am. Mineral. 94 (2009) 827.
[12] L.R. Stieff, T.W. Stern, A.M. Sherwood, Science 121 (1955) 608.
[13] M. Taylor, R.C. Ewing, Acta Crystallogr. B 34 (1978) 1074.
[14] L.H. Fuchs, E. Gebert, Am. Mineral. 43 (1958) 243.
[15] L.R. Stieff, T.W. Stern, A.M. Sherwood, Am. Mineral. 41 (1956) 675.
[16] C. von Keller, Nukleonik 5 (1963) 41.
[17] J.A. Speer, Orthosilicates, in: P.H. Ribbe (Ed.), Mineralogical Society of America, Rev. Mineral. 5 (1980) 113.
[18] B.D. Begg et al., J. Nucl. Mater. 278 (2000) 212.
[19] J. Janeczek, R.C. Ewing, J. Nucl. Mater. 190 (1992) 128.
[20] K. Robinson, G.V. Gibbs, P.H. Ribbe, Am. Mineral. 56 (1971) 782.
[21] A. Meldrum, S.J. Zinkle, L.A. Boatner, R.C. Ewing, Phys. Rev. B 59 (1999) 3981.
[22] A. Meldrum, L.A. Boatner, R.C. Ewing, Mineral. Mag. 64 (2000) 185.
[23] A. Meldrum, S.J. Zinkle, L.A. Boatner, R.C. Ewing, Nature 395 (1998) 56.
[24] W.J. Weber, R.C. Ewing, L.M. Wang, J. Mater. Res. 9 (1994) 688.
[25] V. Pointeau, A.P. Deditius, F. Miserque, D. Renock, U. Becker, J. Zhang, N. Clavier, N. Dacheux, C. Poinssot, R.C. Ewing, J. Nucl. Mater. 393 (2009) 449.
[26] R.E. Williford et al., Nucl. Instrum. Meth. B 141 (1998) 94.
[27] W.J. Weber, R.C. Ewing, C.R.A. Catlow, T. Diaz de la Rubia, L.W. Hobbs, C. Kinoshita, Hj. Matzke, A.T. Motta, M.A. Nastasi, E.H.K. Salje, E.R. Vance, S.J. Zinkle, J. Mater. Res. 13 (1998) 1434.
[28] S.X. Wang, L.M. Wang, R.C. Ewing, Phys. Rev. B 63 (2001) 024105.
[29] S.X. Wang, L.M. Wang, R.C. Ewing, Mater. Res. Soc. Symp. Proc. 504 (1998) 165.
[30] A. Meldrum, L.A. Boatner, R.C. Ewing, Phys. Rev. B 56 (1997) 13805.
[31] J. Lian, K.B. Helean, B.J. Kennedy, L.M. Wang, A. Navrotsky, R.C. Ewing, J. Phys. Chem. B 110 (2006) 2343.
[32] L.W. Hobbs, Nucl. Instrum. Meth. Phys. Rev. B 91 (1994) 30.
[33] L.M. Wang, W.L. Gong, R.C. Ewing, Mater. Res. Soc. Symp. 321 (1994) 405.
[34] J. Lian, L.M. Wang, R.C. Ewing, S.V. Yudintsev, S.V. Stefanovsky, J. Appl. Phys. 97 (2005) 113536.
[35] S.X. Wang, L.M. Wang, R.C. Ewing, K.V. Govindan Kutty, Nucl. Instrum. Meth. B 169 (2000) 135.
[36] A. Meldrum, L.A. Boatner, R.C. Ewing, Nucl. Instrum. Meth. B 141 (1998) 347.
[37] T.D. Shen, S. Feng, M. Tang, J.A. Valdez, Y. Wang, K.E. Sickafus, Appl. Phys. Lett. 90 (2007) 263115.
[38] A.R. Kilmametov, D.V. Gunderov, R.Z. Valiev, A.G. Balogh, H. Hahn, Scripta Mater. 59 (2008) 1027.
[39] J. Zhang, J. Lian, A. Fuentes, F.X. Zhang, M. Lang, F.Y. Lu, R.C. Ewing, Appl. Phys. Lett. 94 (2009) 243110.
[40] E.R. Vance, B.W. Anderson, Mineral. Mag. 38 (1972) 605.
[41] A. Miotello, R. Kelly, Nucl. Instrum. Meth. Phys. Rev. B 122 (1997) 458.
[42] W.C. Butterman, W.R. Foster, Am. Mineral. 52 (1967) 884.
[43] H.R. Hoekstra, L.H. Fuchs, Science 123 (1956) 105.